CrossMark

ORIGINAL PAPER

An Investigation on the Fabric Type Dependency of the Crack Damage Thresholds in Brittle Rocks

E. Ghazvinian · M. S. Diederichs ·
D. Labrie · C. D. Martin

Abstract Fabric-guided micro-fracturing phenomenon in brittle rocks and its effect on crack damage thresholds remains subject to continuing research. The available fabric in rocks can act as a motivator for nucleation and/or extension and interaction of micro-fractures in a preferred orientation, or as a suppressor for growth of micro-cracks in a given direction by different mechanisms such as compliance (stiffness contrast) or preferred orientation of minerals and their boundaries. While anisotropy of brittle rocks in terms of their mechanical strengths can play a significant role in the stability of underground openings, the understanding of the dependency of crack initiation (CI) and crack propagation (CD) thresholds on the available fabric in rocks can improve predictions of the extension and density of micro-fracturing in different directions in the walls of underground openings. To better understand the fabric-guided micro-fracturing phenomenon, and also to study the effect of fabric types available in brittle rocks on their anisotropic behaviour, four types of brittle rocks with different types of fabric are investigated in terms of crack damage anisotropy in this paper. The rocks that are chosen for this study are limestone from the Cobourg Formation, Queenston shale, Olkiluoto mica gneiss and Lac du Bonnet granite. For each rock type, CI and CD thresholds are identified from the unconfined compressive strength testing data. The mechanical behaviour of the four rock types are investigated at each damage stress level and the contributing factors to the isotropic or anisotropic behaviour of the rocks at different crack damage thresholds are discussed.

Keywords Rock mechanics · Brittle rocks, anisotropy · Crack initiation · Crack propagation · Fabric-guided micro-fracturing

E. Ghazvinian (✉) · M. S. Diederichs
GeoEngineering Centre, Queen's University, 36 Union
Street, Miller Hall, Kingston, ON K7L 3N6, Canada
e-mail: e.ghazvinian@queensu.ca

D. Labrie
CanmetMINING, Natural Resources Canada, Ottawa,
ON, Canada

C. D. Martin
Department of Civil and Environmental Engineering,
University of Alberta, Edmonton, AB, Canada

1 Introduction

Anisotropic behaviour can be observed in many rock types at different scales from rock masses to intact rock. While the anisotropy of rock masses is governed by anisotropic faulting, fracturing, jointing, bedding, layering, stratification etc. of the entire rock mass (Amadei 1996), the inherent anisotropic behaviour demonstrated by intact rocks is controlled by similar mechanisms but on a smaller scale (fabric). The term "fabric" is used in this paper as a general term to describe any pre-existing planar feature in intact rock,

for instance, macroscopic foliation, micro-scale layering, preferred orientation of existing micro-cracks, etc.

The anisotropic behaviour of intact rocks in terms of strength and elastic properties has been studied widely by many researchers in the past. This includes studies of the effects of preferred orientation of micro-cracks, foliation, mica content, etc. on the anisotropy of brittle rocks from theoretical, numerical and testing points of view. Early works include studies by Jaeger (1960), Donath (1961), Hoek (1964), Walsh and Brace (1964) and Attewell and Sandford (1974), with more recent works by Gottschalk et al. (1990), Shea and Kronenberg (1993) and Ramamurthy (1993). Most of these studies did not address the influence of fabric on the onset of crack initiation thresholds (CI), or guiding the fracturing at the cracks interaction and propagation stress level (CD).

The in situ behaviour of brittle rocks around deep underground excavations can be predicted more accurately with recent developments in understanding the mechanical damage and micro-mechanics of failure in brittle rocks (Martin 1997; Diederichs 2003, 2007). A better understanding of the effect of anisotropy on the onset of CI and crack propagation thresholds can improve the prediction of the micro-fracturing behaviour of massive brittle rocks containing a fabric around underground openings. While the works such as those presented in Gatelier et al. (2002), Colak and Unlu (2004), Hakala et al. (2005), Nicksiar and Martin (2013), Amann et al. (2014) and Ündül et al. (2015) address fabric guided fracture growth and strength dependence, this study further improves the understanding of the dependency of the onset of crack damage thresholds in intact brittle rocks containing a fabric to the fabric orientation and the fabric type, (e.g. foliation, micro-scale layering, preferred orientation of pre-damage etc.). For this purpose, four different types of brittle rocks with different types of fabric are investigated. Detailed analyses were carried out on the unconfined compressive strength (UCS) testing results of the four rock types to investigate the existence of fabric-guided micro-fracturing phenomenon and its effect on the crack damage thresholds.

2 In Situ Strength of Brittle Rocks: Damage Thresholds

Spalling is a failure mechanism that is commonly observed in the walls of underground excavations in brittle rocks (low ratio of tensile to compressive strength). The spalling strength of massive to moderately jointed brittle rock masses under low confinement is considerably lower than the peak strength measured in the laboratory (Martin et al. 1999; Diederichs 2003). Spalling occurs through the initiation of fractures parallel to the excavation boundary. The formation of a notch is by fracture propagation and coalescence under higher induced stresses or stress corrosion and fatigue. The feedback confinement due to the hoop tension caused by the geometrical boundary conditions in laboratory compressive tests suppresses the propagation of the dilated fractures and therefore intensifies the estimated failure stress (Peng 1971; Peng and Johnson 1972; Diederichs 2007). Lower and upper in situ strength limits can be defined for brittle rocks according to the damage thresholds. The upper bound or short term in situ strength tends to follow the yielding limit of the rock and corresponds to the onset of crack propagation or the Critical Damage threshold (CD). The lower bound or the ultra long-term in situ strength of brittle rocks is coincident with the onset of the CI threshold (Diederichs 2007). It is shown by Brace et al. (1966) and Bieniawski (1967) that the onset of non-linearity of axial strain and lateral strain plotted versus axial stress corresponds well to the CD and CI thresholds, respectively (Fig. 1).

2.1 Estimation of Crack Damage Thresholds in the Laboratory

Spalling does not occur in laboratory rock samples as previously mentioned due to the geometrical boundary
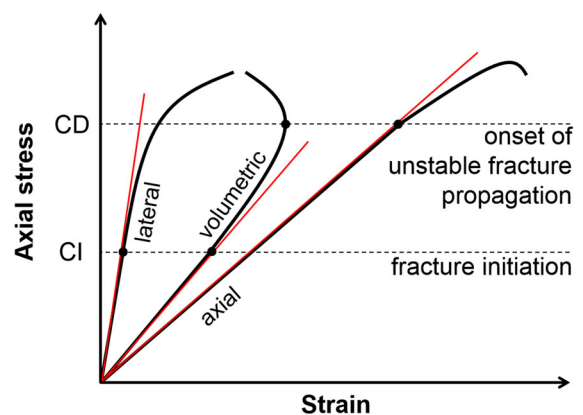

Fig. 1 Crack damage stress levels for a brittle rock specimen (after Bieniawski 1967)

condition. Therefore direct measurement of CI and crack propagation thresholds is impractical with a conventional UCS testing procedure. Rigorous strain measurement or acoustic emission (AE) monitoring of laboratory compressive tests are currently the two most practical means for determination of CI and CD. A detailed study of the different methods for laboratory estimation of crack damage thresholds can be found in Ghazvinian et al. (2012a).

Crack initiation, propagation and grain boundary sliding in rocks can create AE pulses (Obert 1977). A relationship can be established between the increasing rate of AE activity in brittle rocks and crack damage progression. Estimation of CI and CD from AE data is schematically illustrated in Fig. 2a. The axial stress that corresponds to the first instance of the sudden increase in the crack intensity or cumulative number of AE events above the background noise is identified as the onset of CI for the rock. The typical linear increase in the AE activity before CI as observed in Fig. 2a is attributed to the background noise level, which is assumed to remain constant during the tests. The next stress threshold after CI where the crack intensity plot deviates from linearity corresponds to CD (Diederichs et al. 2004).

Martin (1997) suggested using the crack volumetric strain (ε_{CV}) for estimation of the CI threshold to reduce the uncertainty associated with measuring CI at the onset of non-linearity in the axial stress–lateral strain curve. Volumetric and crack volumetric strains can be calculated from the collected axial (ε_{axial}) and lateral ($\varepsilon_{lateral}$) strains during a laboratory compressive test. In this approach, as illustrated in Fig. 2b, CI is identified as the maximum point of crack volumetric strain and CD is estimated as the reversal point of volumetric strain.

For a cylindrical rock sample, the volumetric strain (ε_{Vol}) is calculated as:

$$\varepsilon_{Vol} = \varepsilon_{axial} + 2\varepsilon_{lateral} \quad (1)$$

and the crack volumetric strain is calculated as the difference between the volumetric strain and the elastic volumetric strain (ε_{EV}) as:

$$\varepsilon_{CV} = \varepsilon_{Vol} - \varepsilon_{EV} \quad (2)$$

and the elastic volumetric strain is given by:

$$\varepsilon_{EV} = \frac{1 - 2v}{E}(\sigma_1 - \sigma_3) \quad (3)$$

where E and v are the Young's modulus and Poisson's ratio, respectively, and σ_1 and σ_3 are the major and minor principal stresses.

The advantages and disadvantages of the described methods for estimation of damage thresholds are discussed in detail in Ghazvinian et al. (2012a). In this paper the crack damage stress levels for the tested rocks are estimated by both the AE and strain methods where possible.

3 Anisotropy Models

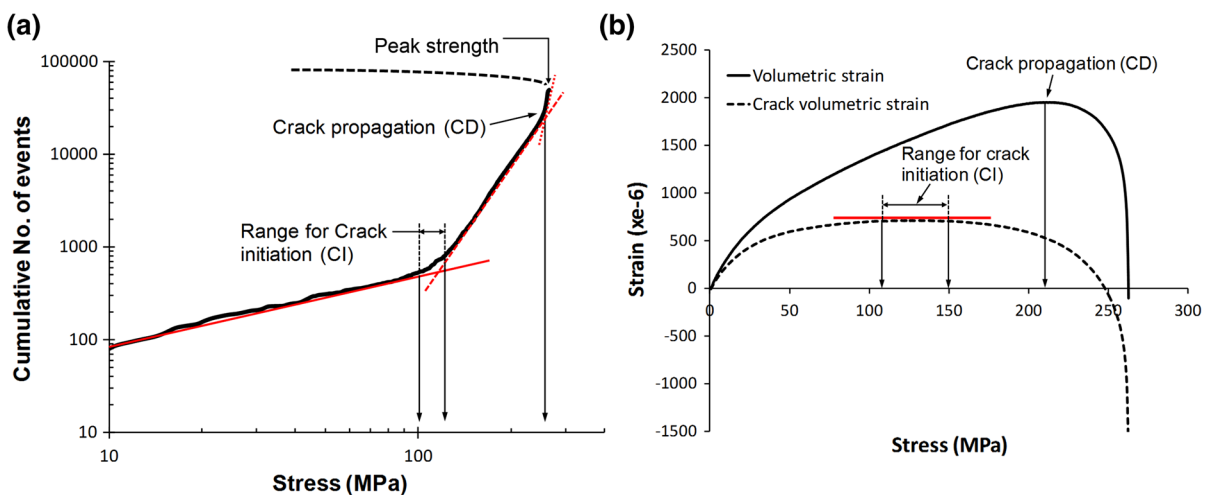Several modes of macroscopic response can be assumed for intact rocks that consist of a fabric. Based

Fig. 2 Identification of crack damage thresholds by using **a** the AE method, **b** the strain method

on the data collected and the anisotropy models proposed by previous researchers (Jaeger 1960; Donath 1961; McLamore and Gray 1967; Pariseau 1972; Karr et al. 1989; Gottschalk et al. 1990; Shea and Kronenberg 1992), the orientational strength dependence of intact rocks containing fabric is summarized in Fig. 3. In the simplest form (Fig. 3a), the fabric is defined as a unique plane of weakness (Jaeger 1960). Jaeger's "plane of weakness" theory was originally developed to describe the shear strength of intact rock cut by a single joint or a joint set, but then for simplicity, the developed classical U-shape curve was applied to describe the inherent anisotropy of intact rocks. In transversely anisotropic models (Fig. 3b) the continuous variation of shear strength is predicted as a function of the relative orientation between the fabric and the major principal stress axes or the more general orientations that do not necessarily strike parallel to the fabric plane (Jaeger 1960; McLamore and Gray 1967; Pariseau 1972; Karr et al. 1989; Gottschalk et al. 1990). There are also some exceptions that deviate from the general assumption that all rocks that consist of a fabric are anisotropic by demonstration of isotropic behavior [e.g. a few types of mica-rich rocks studied by Shea and Kronenberg (1992)], as shown in Fig. 3c.

The fabric arrangement in rocks directly influences their anisotropic response and different modes of behaviour as shown in Fig. 3 (Gatelier et al. 2002). The planar arrangement of textural and/or structural features in intact rocks can be represented by one of the fabric elements shown in Fig. 4. The difference in mineral composition (Fig. 4a), preferred orientation of platy minerals and grain boundaries (Fig. 4b–c), spatial variation of grain sizes (Fig. 4d), preferred orientation of platy minerals, lenticular mineral aggregates or planar micro-fractures in an isotropic matrix (Fig. 4e–g) or the combination of any of these
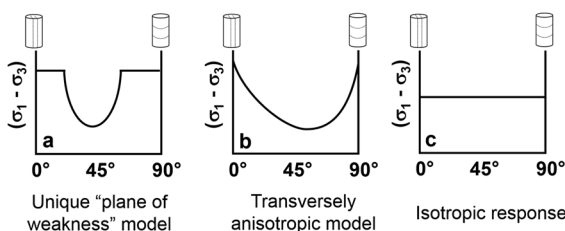
fabric elements (Fig. 4h) can introduce anisotropical effects to the mechanical behaviour of these intact rocks (Passchier and Trouw 2005).

The described anisotropy models for orientational strength dependence in Fig. 3 can be employed for describing the fabric-guided micro-fracturing phenomenon in intact brittle rocks. In general the preferred orientation of induced micro-fracturing in intact brittle rocks can occur in two general circumstances:

- *Mineralogical-related* lamination in rock or preferred orientation of minerals within the intact rock.
- *Stress-induced* high deviatoric stress conditions (with respect to the strength of the rock) can induce micro-fracturing parallel to the orientation of major principal stress. For example, this occurs due to relaxation (stress relief cracking) of brittle rocks or drilling-induced micro-fracturing due to the stress concentration in the proximity of well bore bottom in the rock. Under sufficient stress concentrations and particular stress orientations, the micro-fracturing from the high induced tensile stress within the rock can lead to core discing (Jaeger and Cook 1963; Obert and Stephenson 1965; Stacey 1982; Dyke 1989; Li and Schmitt 1998).

This is also in agreement with Barla's (1974) general classification of rock anisotropy. Barla (1974) distinguishes rocks that exhibit anisotropic behaviour into two groups: Class A, those with apparent isotropy (anisotropic behaviour can be due to the preferred orientation of pre-existing damage in rock) and Class B, those with clear evidence of mineralogical fabric in the rock.

4 Experimental Methodology

Four types of brittle rocks exhibiting different types of planar fabric (including rock types with class A and B according to Barla's (1974) classification) were chosen to be investigated to determine the effect of fabric orientation on the critical stress levels in this study. The chosen rocks were the Cobourg limestone, Lac du Bonnet granite, Queenston shale and Olkiluoto mica gneiss.
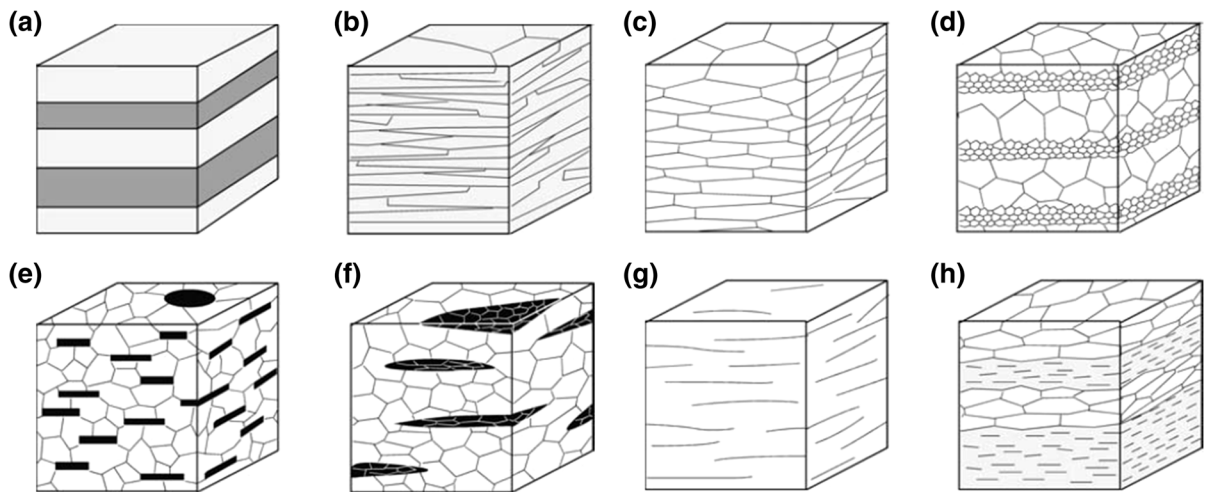

Fig. 3 Anisotropy models describing the orientational strength dependence for intact rocks consisting of a fabric

Fig. 4 Fabric elements that introduce planar anisotropy in intact rocks (after Passchier and Trouw 2005, modified from Hobbs et al. 1976)

4.1 Rock Types

4.1.1 Cobourg Limestone

The Cobourg limestone Formation, which is Middle to Upper Ordovician in age, is a relatively thin unit of the Trenton Group. It is found in the Michigan Sedimentary Basin and is part of a large limestone package which marks a depositional environment transition from a restricted coastal to a shelf environment (Mazurek 2004). A similar depositional environment existed in the Appalachian Sedimentary Basin (which was connected to the Michigan Basin). The Cobourg Formation is also known as the Lindsay Formation in south-central and eastern Ontario (Darlington Nuclear Power Station to Ottawa; Gartner Lee 2008). The Cobourg is an argillaceous limestone which is light gray in colour and contains dark gray argillaceous wisps and inclusions which loosely mark the irregular bedding. This feature is likely due to bioturbation and/or compaction during diagenesis. Typically the argillaceous 'bedding' grades into or abruptly changes to light gray fossiliferous limestone. The apparent anisotropy in this rock is governed by the depositional sequences, with alternating layers of fossil rich packstone and lime-mudstone bands (Fig. 5a). The preferred orientation of nodules in the limestone bound by the dark grey wisps and inclusions (fine-grained limestone with argillaceous content) is clearly evident in samples with dimensions larger than

approximately 0.25 m. These nodules are similar in size to laboratory scale specimens and are therefore occasionally difficult to identify in a typical cylindrical specimen with diameter ranging between 50 and 60 mm. At this scale the dark grey inclusions can appear undulating and discontinuous and therefore represent heterogeneity in the Cobourg limestone. The effect of scale, heterogeneity and rock fracturing strength is discussed in detail in Sect. 6.1.1.2.

4.1.2 Lac du Bonnet Granite

Canada's former Underground Research Laboratory (URL) for investigation of nuclear waste disposal in plutonic rocks is situated within the granite of the Lac du Bonnet batholith, in Southeastern Manitoba, Canada. The Lac du Bonnet batholith, dated back to late Kenoran (2680 ± 81 Ma), is elongated ENE-WSW approximately 75 by 25 km and is about 10 km in depth in the Winnipeg River plutonic complex of the English River gneiss belt (Read and Martin 1996). The batholith is composed of massive, medium- to coarse-grained porphyritic granite that exhibits relatively uniform texture and composition over the batholith with local subhorizontal gneissic banding (Everitt et al. 1990).

In situ stress measurement were performed extensively at the URL. From over 1000 overcoring measurements, 80 hydraulic fracturing tests, and in situ stress determination from back calculation of
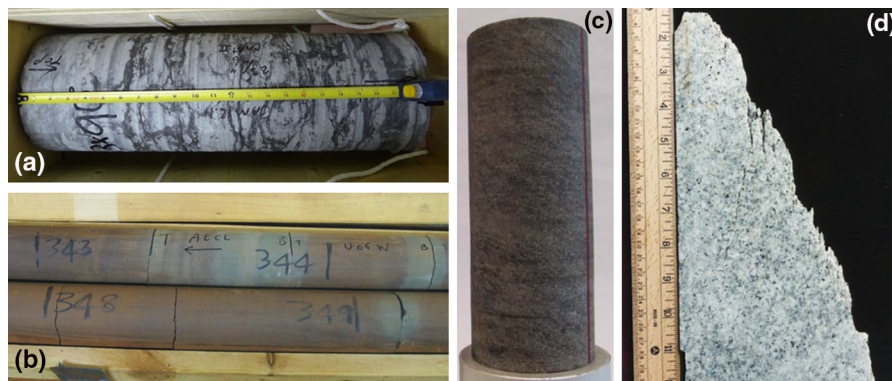
Fig. 5 Samples of **a** Cobourg limestone, **b** Queenston shale, **c** Olkiluoto mica gneiss and **d** grey Lac du Bonnet granite (after Martin 1993)

convergence measurements (Martino et al. 1997), the in situ stress tensor for Level 420 was determined as presented in Table 1. At Level 420, the stresses are relatively high in comparison to the maximum principal stresses measured at the same depth elsewhere in the Canadian Shield (Fig. 6; Martino and Thompson 1997).

Sample disturbance is an inevitable artifact when obtaining samples from a high stress environment. The induced micro-cracking within the intact rock can be due to coring (stress concentration) or relaxation (unloading or de-stressing) or as a combination of both. At the 420 Level due to the high in situ stress, sample disturbance and in the extreme case, core discing was observed for core samples ranging from 18 mm to 1.25 m in diameter, with disc thickness varying from a few mm to several cm (Martin 1993).

Table 1 Best estimate of the in situ stress tensors (from Martin et al. 1997) and the mechanical strength properties of the grey granite from the 420 Level of the URL (from Eberhardt 1998)

Stress components	σ_1	σ_2	σ_3
Magnitude (MPa)	60 (±3)	45 (±4)	11 (±4)
Trend/plunge (°)	145/11	054/08	290/77
Stress ratios	σ_1/σ_2	σ_1/σ_3	σ_2/σ_3
	1.33	5.45	4.10
Strength parameters	420 m level grey granite		
CI (MPa)	76.4 (±3.7)		
CD (MPa)	100.4 (±12.2)		
UCS (MPa)	157.1 (±17.7)		

Standard deviation in parentheses

The sample disturbance drastically influenced the peak compressive strength of the samples obtained from the 420 Level in comparison to the samples recovered from the 240 Level and above, that were tested in the laboratory (Read and Martin 1996). Mechanical properties of the Lac du Bonnet granite and the associated damage and core discing at depth have been investigated extensively, such as the work documented in Martin (1993), Eberhardt (1998), Everitt (2001) and Lim and Martin (2010). The strength properties of the grey Lac du Bonnet granite from the 420 Level of the URL are listed in Table 1. The fabric in the Lac du Bonnet granite specimens from the 420 Level that are studied in this paper is defined by the stress-induced micro-fractures with preferred orientation.

4.1.3 Olkiluoto Mica Gneiss

Mica gneiss is one of the dominant rock types at the proposed Finnish site for its used nuclear fuel repository in Olkiluoto, Finland (Hakala et al. 2005). The main minerals for this rock are classified as fine to medium grained quartz, potassium and biotite. The thin section study of the mica gneiss at Olkiluoto borehole OL-KR10 showed that biotite, quartz and feldspar make up at least 77 % of all minerals, and the average mica content of samples from different depths is over 20 % (Hakala and Heikkila 1997). The Olkiluoto mica gneiss is clearly foliated and typically metamorphous and therefore is anticipated to exhibit anisotropic behaviour (Vaittinen et al. 2003; Hakala et al. 2005). The foliation in a laboratory specimen of the Olkiluoto mica gneiss is shown in Fig. 5c.
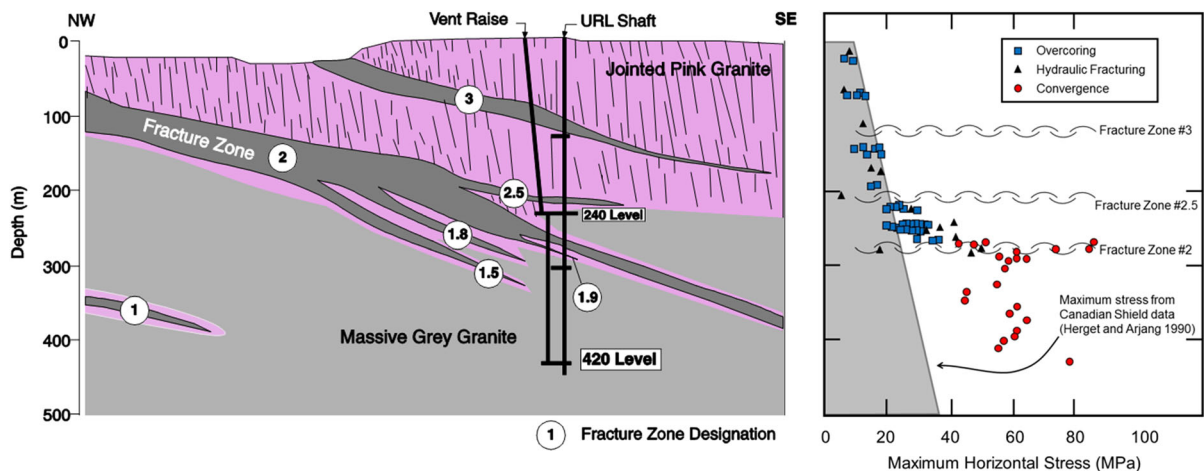
Fig. 6 Generalized geology and the in situ stress measurements at the URL (after Thompson and Chandler 2004)

4.1.4 Queenston Shale

The Queenston Formation is part of the sedimentary secession of the Appalachian and Michigan sedimentary basins and is Upper Ordovician in age. It can include interbeds of siltstone, sandstone and fossiliferous carbonates and regionally grades from coarse to fine grained in a north westerly direction, away from the sediment source on the east coast of North America (Brogly et al. 1998). In the Niagara region, where the testing samples came from, the formation is predominately mudstone to silty mudstone (Fig. 5b; Rigbey et al. 1994). The rock mass appears massive, but bedding is visible in thin sections representing alternating depositional layers of similar minerals, which in decreasing order of abundance are typically quartz, muscovite, chlorite, calcite and illite (Schandl 2009; Perras 2009).

The Cobourg limestone and the Olkiluoto mica gneiss fall within class B of Barla's (1974) classification by demonstration of mineralogical fabric. The investigated Lac du Bonnet granite and Queenston shale specimens are categorized as Barla's (1974) class A rocks, since the fabric in these rocks only appears at the micro-scale.

5 Laboratory Testing

Anisotropy of the four rock types in terms of their CI, CD and peak unconfined strength is investigated through the study of the UCS test data for specimens with several different fabric orientations.

The Cobourg limestone specimens were drilled from large cores (200 mm diameter) that were obtained from a quarry in Bowmanville, Ontario, courtesy of the Nuclear Waste Management Organization of Canada (NWMO). The specimens were prepared for testing with an average diameter of 54 mm and a length to diameter ratio of approximately 2.2, resulting in 5 sets of specimens with different fabric (apparent bedding) orientations which are 0°, 30°, 45°, 60° and 90° with respect to the loading axis. An example of the drilling process and specimens with different fabric orientations for the Cobourg limestone are shown in Fig. 7. The specimen fabric orientations are measured with respect to the direction of loading. The fabric orientation measurement scheme will remain the same for the other rock types investigated in this paper.

For each fabric orientation set, six specimens were prepared and tested for UCS according to the ISRM (1999) and ASTM (2012) suggested methods. Loading of the specimens was conducted in axial strain control mode (0.00059 mm/s) and specimen deformation data was collected by using two opposing axial and two lateral strain gauges for four out of the six specimens. For the two remaining specimens in each orientation set, linear variable differential transformers (LVDTs) and extensometers connected to a chain wrapped around the specimens were used for the axial and circumferential deformation measurements, respectively. The AE activity of the specimens was recorded

during the tests by means of a Physical Acoustics Corporation (PAC) Pocket AE and two PAC R15 AE transducers. The UCS testing setup for the Cobourg limestone is shown in Fig. 8a.

In addition to testing the UCS of the Cobourg limestone, the change of the tensile strength of this rock with respect to the fabric orientation was measured from indirect tensile strength (Brazilian) tests. The Brazilian disks were cut from the core just above and below the location of the UCS specimens with an approximate thickness of 40 mm to satisfy the requirements of the ISRM (1978) suggested method for determining tensile strength of rock materials. The Brazilian disks were grouped in the same fabric orientation set as the cylindrical specimens from which they were cut. The Brazilian tests were conducted with a loading rate of 0.11 kN/s with three different loading angles (δ) of 0°, 45° and 90° for each fabric orientation set. The 45° Brazilian disks prepared for testing and the schematic representation of the different fabric orientations and loading angles for the Brazilian specimens are shown in Fig. 9.

The crack damage thresholds and peak compressive strength data for the Olkiluoto mica gneiss were determined by Hakala et al. (2005). Nineteen UCS specimens with fabric orientation ranging from 10° to 90° were tested. AE data was collected for all the specimens and deformation was simultaneously monitored by means of strain gauges and extensometers
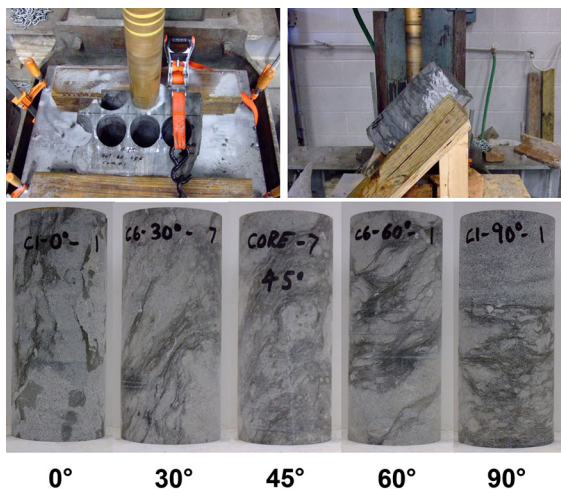

Fig. 7 *Top* drilling of 54 mm diameter specimens with different orientations from large Cobourg limestone core samples. *Bottom* prepared Cobourg limestone specimens with different fabric orientations

(Fig. 8b). The reader is encouraged to consult Hakala et al. (2005) for a detailed description of the test setup and specimen selection process.

The UCS test data for the Lac du Bonnet granite was provided courtesy of CanmetMINING, Natural Resources Canada from their testing program that was performed for Atomic Energy Canada Limited (AECL) in the 1980s and 1990s. The testing was part of a research program to investigate the anisotropy of the Lac du Bonnet granite in terms of its uniaxial mechanical properties. To focus on the effect of pre-existing preferential orientated micro-cracks on guided micro-fracturing and crack damage anisotropy, the studied specimens are limited to the grey Lac du Bonnet granite from the 420 Level. Four 200 mm diameter cores were obtained from a borehole with dip of $-2.1°$ and strike of $67°$ at the 420 Level. Twelve 45 mm diameter specimens with an approximate length of 100 mm were drilled from each of the 200 mm cores with different orientations. The 48 resulting specimens were classified according to their orientations with respect to the axis of the large cores. The orientation of the 45 mm specimens with respect to the large cores' axes were measured with angle 'β', location of the collar of the 45 mm hole around the circumference of the 200 mm core and angle 'α', the angle between core axes of the 45 mm specimen and the 200 mm core, as illustrated in Fig. 10. The 45 mm specimens were drilled from the large diameter cores with various α and β orientations: 0°, 22.5°, 45°, 67.5° and 90°.

UCS testing of the Lac du Bonnet granite specimens was performed in load control mode, loading the specimen to failure within approximately 3 min. Deformation of the specimen was measured by two opposing axial and two opposing lateral strain gauges. The two strain gauges for measurement of deformation in each direction were connected in series to form a single active strain gauge.

The Queenston shale UCS test data was obtained courtesy of Ontario Power Generation (OPG) from tests that were completed previously at the design stages of OPG's Niagara Tunnel Project. The Queenston shale testing data used in this study are from specimens originating from a borehole under St. David's Gorge in the Niagara region. The specimens were taken from depths ranging between 203 and 236 m below the ground surface. The data was filtered to select only those tests conducted on specimens at their natural in situ moisture content to minimize the
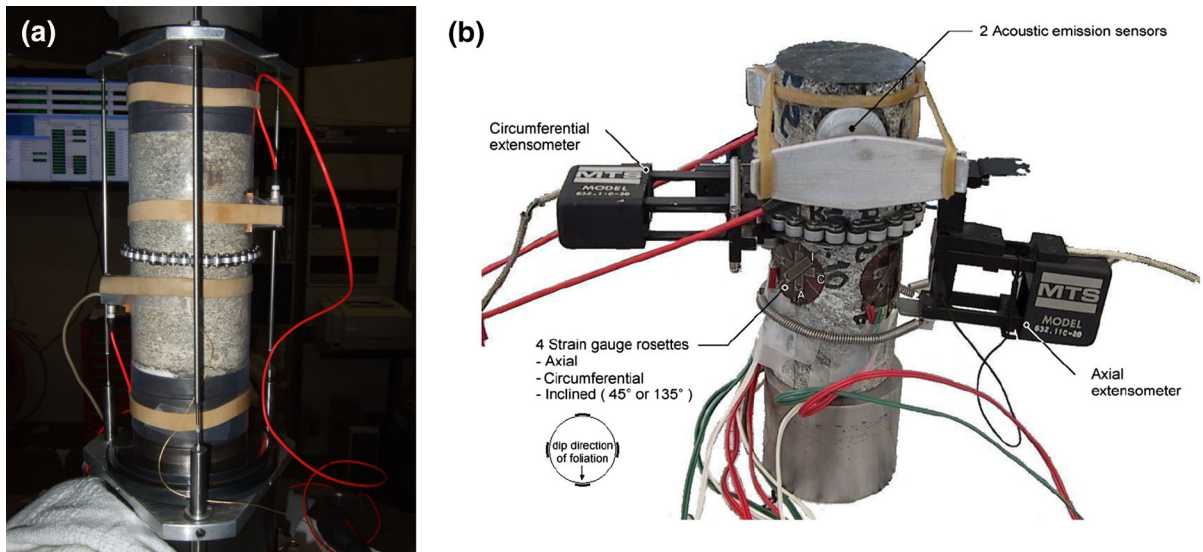
Fig. 8 UCS test setup for **a** the Cobourg limestone and **b** the Olkiluoto mica gneiss (from Hakala et al. 2005)
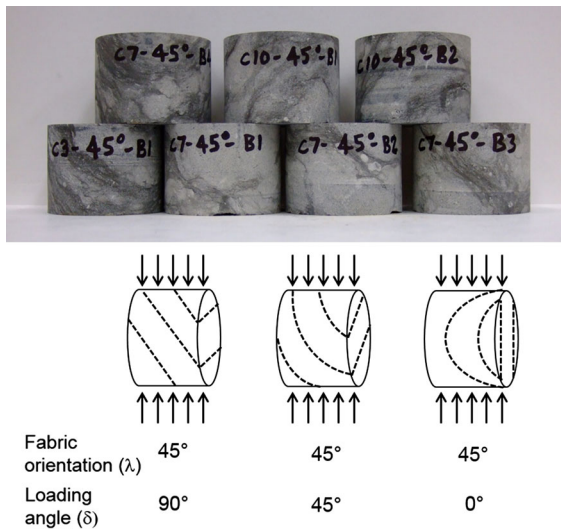

Fig. 9 *Top* samples of 45° Brazilian specimens, *Bottom* schematic illustration of three different loading angles for a Brazilian specimen with 45° fabric orientation
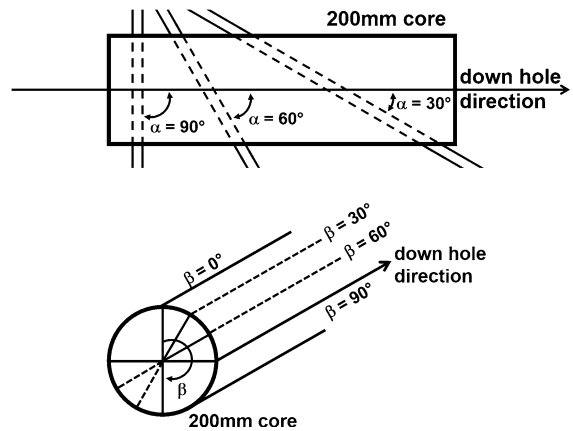

Fig. 10 Drilling of 45 mm Lac du Bonnet granite specimens from large diameter cores and the illustration of varying α and β orientations

influence of sample disturbance. After filtering, the data set included testing data for 4 specimens that were drilled parallel to the bedding (0°), 4 specimens oriented at 45° to the bedding and 15 specimens drilled perpendicular to the bedding (90°). Deformation data of the 0° and 90° specimens was collected with axial and lateral strain gauges while the deformation data of

the 45° specimens was only measured by axial strain gauges. Therefore only the peak strength of the 45° specimens is included in the fracturing strength anisotropy evaluation of the Queenston shale.

6 Test Results

The measured mechanical properties for specimens of the four rock types are summarized in this section.

6.1 Cobourg Limestone

6.1.1 UCS and Damage Thresholds

The measured peak unconfined strengths for the Cobourg limestone specimens belonging to the five sets of specimens with different fabric orientations are presented in Fig. 11. The onset of CI and CD thresholds for the Cobourg limestone was identified by means of both the AE and the strain method. Estimation of CI and CD thresholds from the strain approach was from the stress associated with the maximum crack volumetric strain and volumetric strain, respectively. These results are shown in Fig. 11 and listed in Table 2. No formal significance should be placed in the best fit second degree polynomial functions used to capture the sensitivity of stress limits to the fabric orientation.

The authors are more confident in the CI and CD trends for anisotropy that is established from the AE data, in comparison to the strain method. This is mainly due to the use of strain gauges (four out of six specimens for each orientation) for the deformation monitoring of the Cobourg limestone. Identification of CI and CD with strain gauge data can be impossible or erroneous for the Cobourg limestone tests, due to the layering and heterogeneity that exists at the laboratory specimen scale, which can lead to local (in the vicinity of the strain gauge) rather than global deformation measurement.

6.1.1.1 Failure Mode The failure mode for each of the Cobourg limestone specimens (axial splitting versus shearing or a mixed mode) was identified in the laboratory after each test. The results are shown in Fig. 12. While axial splitting is observed to be the dominant failure mode for the 0° and 90° specimens, the 30°, 45° and 60° specimens are seen to fail in mixed mode or shearing. Shear failure along the so-called "weak fabric planes" in the 30°, 45° and 60° specimens masks the crack propagation threshold effect on the volumetric strain (the axial stress–volumetric strain plot never reaches a turning point). Therefore as seen in Fig. 11, CD from the strain method could only be identified for a limited number of specimens.

6.1.1.2 Heterogeneity and Scale Effect The relatively wide distribution of UCS, CI and CD thresholds measured for the Cobourg limestone samples within each fabric orientation set can be attributed to the
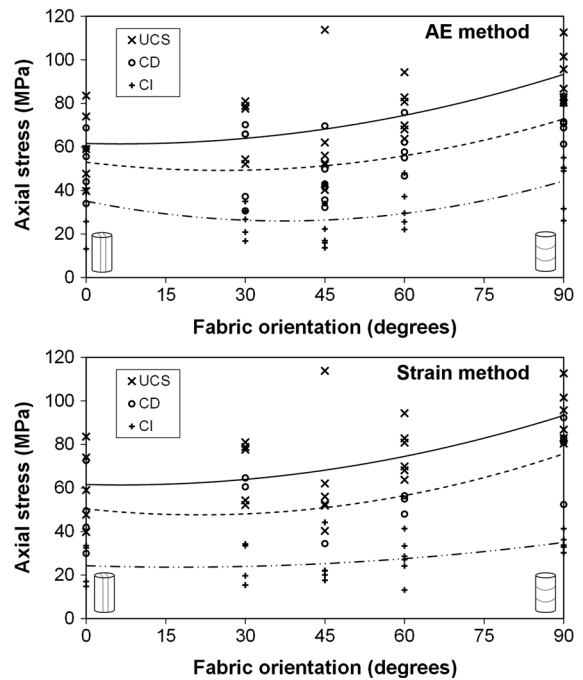

Fig. 11 UCS and CI and CD thresholds estimated from the AE and strain methods for the Cobourg limestone (the *trend lines* are second degree polynomial fit)

heterogeneity that is inherent in the Cobourg limestone at the laboratory specimen scale. Although the wisps and inclusions observed in the Cobourg limestone laboratory samples appear to be heterogeneous, a visual examination of larger samples of the Cobourg limestone (40 cm cubes) demonstrate a more homogenous nature. Therefore it is anticipated that a more uniform distribution of strength and crack damage thresholds can be obtained by testing larger samples.

To investigate the effect of heterogeneity on the peak strength of the Cobourg limestone, the approximate ratio of the compositional dark wisps (fine-grained limestone with argillaceous content) to the entire volume of the specimens was estimated by means of simple image processing technique. For this purpose ImageJ (Schneider et al. 2012), a public domain image processing software, was used. The percentage of the composing dark grey wisps for each specimen was approximated as the average of the percent of the dark grey area from two pictures taken on two opposing sides of each specimen. The simplified procedure is shown in Fig. 13, in which the specimen picture is imported into ImageJ (Fig. 13a), the threshold for estimation of the grey areas is

Table 2 The mean measured UCS, CI and CD thresholds estimated from the AE and strain methods for the Cobourg limestone specimens

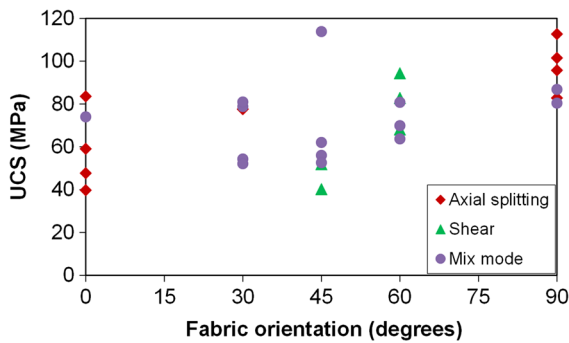| Fabric orientation (°)	UCS (MPa)	AE method		Strain method	
		CI (MPa)	CD (MPa)	CI (MPa)	CD (MPa)
0	60.8	35.5	52.3	24.5	48.5
30	68.8	26.0	54.0	23.7	62.5
45	62.8	24.4	45.3	25.2	34.4
60	76.6	32.5	59.5	28.0	53.1
90	93.3	43.8	72.6	34.9	77.1

Fig. 12 Failure modes of the Cobourg limestone UCS specimens

calibrated (Fig. 13b) and finally the ratio of black (dark grey areas) versus white (light grey areas) pixels is estimated (Fig. 13c). The sensitivity of UCS, CD and CI to this ratio are shown in Fig. 13d–f. A general trend can be established between the ratio of the composing fine-grained lime-mudstone wisps and inclusions (dark grey) and coarser-grained packstone (light grey) with the fracturing strengths for Cobourg limestone. Increasing this ratio decreases the UCS, CD and CI. The percentages of the dark grey wisps in larger Cobourg limestone samples are anticipated to be within a narrow range and therefore the effect of heterogeneity on the variation of the peak and CI and CD thresholds should be minimal.

6.1.2 Elastic Constants

The Young's moduli and Poisson's ratios for the Cobourg limestone specimens were calculated over a range of 30–50 % of the peak strength, to minimize the effect of micro-fracturing on the calculation of the elastic responses. The calculated elastic constants for the specimens with different fabric orientations are demonstrated in Fig. 14. These values were used for

calculation of the crack volumetric strain and therefore estimation of CI through the strain approach.

The mean Young's moduli for different fabric orientations represent a bi-modal distribution, with the maximum value occurring at 30° and the second maximum at 60°. This bi-modal distribution can be due to the presence of a secondary preferred micro-fracturing plane as described by Barron (1971). However, since this behaviour is not observed in the strength plots or the Poisson's ratio envelope, it is more likely to be an inconsistent behaviour in specimens with a 45° fabric orientation. A significant trend cannot be established between the fabric orientation and the mean Poisson's ratios, however; the maximum mean Poisson's ratio is observed (Fig. 14) to occur for specimens with the fabric oriented at 30°, similar to the maximum Young's modulus.

6.1.3 Tensile Strength

The tensile strength of the Cobourg limestone, as measured from the Brazilian testing of specimens with different fabric orientations at various loading angles, ranged between 3.0 and 10.4 MPa. The fracturing patterns of the Brazilian disks are shown in Fig. 15 and the tensile strengths and the mean distribution for various fabric orientations and loading angles are shown in Fig. 16. Since rotation of the 90° specimens around their central axes does not change the loading angle (δ in Fig. 9), the same test results are repeated at the various loading angles for the 90° fabric orientation in Fig. 16. The loading angle is observed to play an important role on the measured tensile strength when comparing the tensile strengths of specimens tested at a 0° loading angle (increasing trend with increasing fabric orientation) with samples tested at a 90° loading angle (bi-modal distribution). The change in loading angle in Figs. 15 and 16 appears to control the degree of fabric involvement in the failure of the
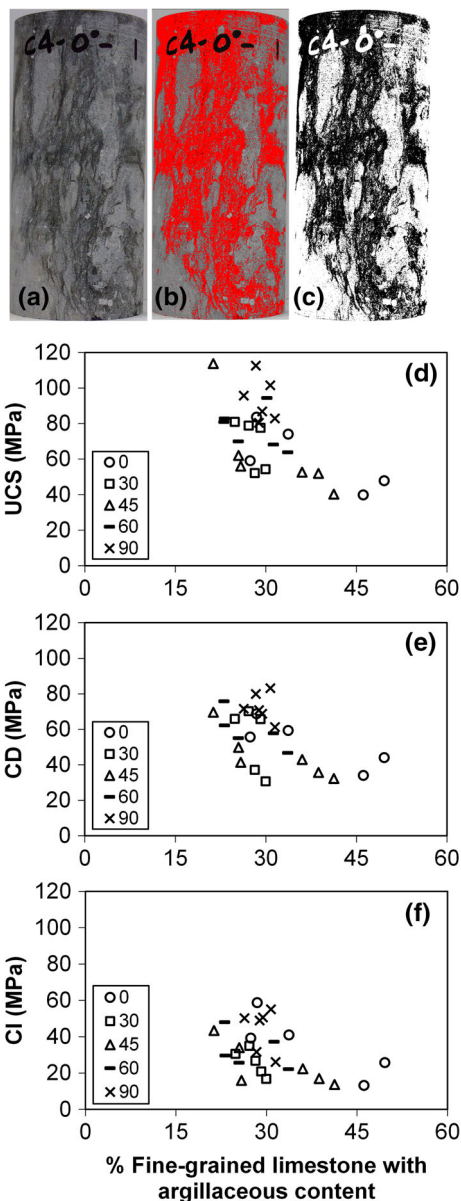
Fig. 13 Heterogeneity study for the Cobourg limestone, **a** an example of a Cobourg limestone specimen used for estimating the percent of composing dark grey argillaceous inclusions, **b** calibrating the threshold for estimation of the *dark grey areas*, **c** measurement of *black* versus *white* pixels which represent the dark grey inclusions and the light grey matrix of the Cobourg limestone, respectively, **d**–**f** the correlation between the fracturing stress limits and the percentage of the composing dark grey argillaceous inclusions in the Cobourg limestone specimens

specimens consistent with Dan et al. (2013) Brazilian tests on Gneiss and Slate. Further testing with a larger number of samples is required to better understand the

effect of the loading angle in combination with the fabric orientation on the failure mechanism of Brazilian samples and consequently the tensile strengths.

6.2 Lac du Bonnet Granite

The CI and CD thresholds for the Lac du Bonnet granite specimens were estimated from the strain data only, due to the absence of AE activity monitoring. The crack propagation threshold for the specimens was estimated from the reversal point of the volumetric strain, while the CI threshold was estimated from the maximum crack volumetric strain, and also from the onset of non-linearity (or change in curvature) of the lateral strain. Testing of the Lac du Bonnet granite specimens drilled from the large 20 cm cores, with a wide variety of orientations, allowed for investigation into the effects of preferred orientation of pre-existing damage in the rock due to drilling and the likely stress relief cracking effect on the fabric-guided micro-fracturing phenomenon.

6.2.1 Drilling-Induced Damage

Two sets of specimens were drilled at perpendicular directions with 90° offset from each other ($\beta = 0°$ and $\beta = 90°$) to the circumference of the large (20 cm) Lac du Bonnet granite cores with various α orientations. Assuming that the drilling damage to the large cores occurred perpendicular to the direction of drilling, the orientation of "α" for the specimens from these two sets of specimens will be identical to the orientation of the fabric (preferred orientation of pre-existing micro-cracks). Therefore the mechanical response of these specimens is suited for studying the drilling-induced damage effect on the fabric-guided micro-fracturing. The test results are shown in Fig. 17 and listed in Table 3. The second degree polynomial fits to the data are also illustrated in this figure. The elastic constants in Fig. 17 are the tangent modulus and Poisson's ratio calculated at 40 % of the peak strength for the specimens. The relatively high values for the Poisson's ratio can be attributed to the pre-existing damage in the rock.

6.2.2 Relaxation-Induced Damage

The major principal stress is horizontal and the minor principal stress is vertical with the σ_1/σ_3 ratio

Fig. 14 Calculated elastic constants for the Cobourg limestone, *left* Young's modulus, *right* Poisson's ratio (the mean values at each orientation are connected by the *red lines*)
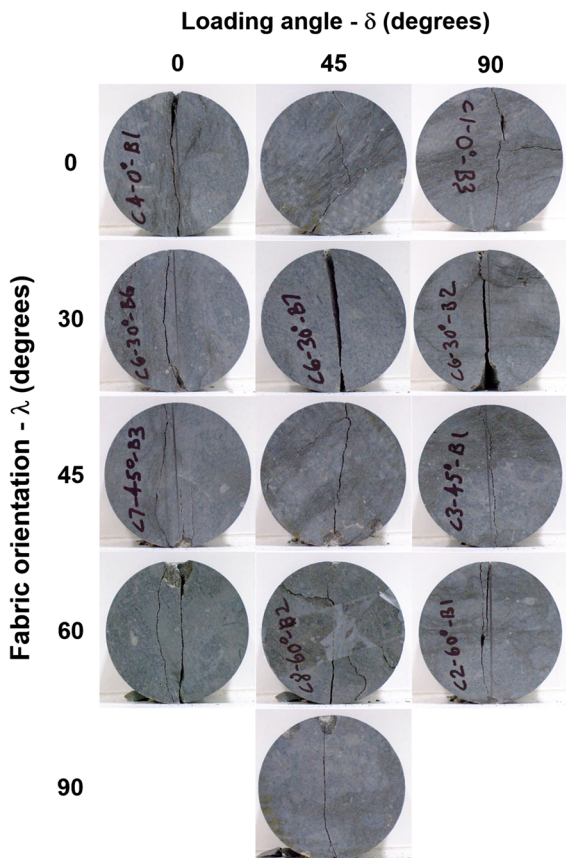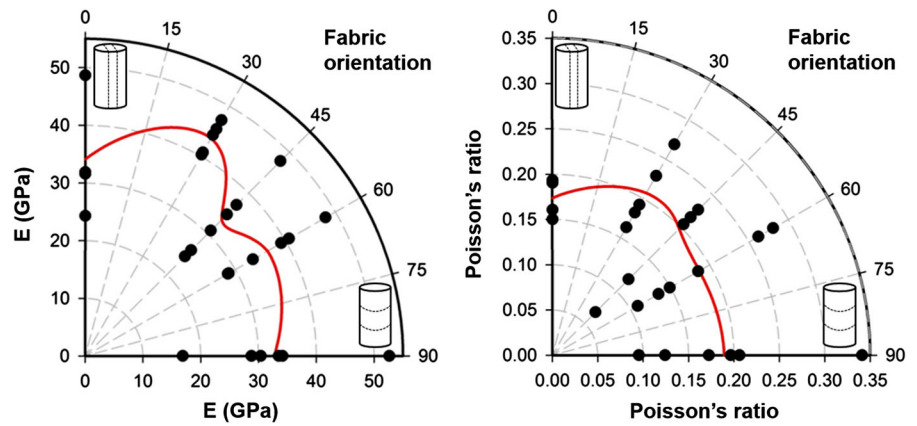

Fig. 15 The effect of the fabric orientation and the loading angle on the fracture pattern of Cobourg limestone Brazilian specimens

Fig. 16 The tensile strengths and the mean distribution for the Cobourg limestone Brazilian disk specimens with different fabric orientations tested with various loading angles

are drilled perpendicular to the circumference of the large cores ($\alpha = 90°$) are therefore used to study the effect of relaxation-induced preferentially orientated damage on the fabric-guided micro-fracturing. The orientation of the laboratory specimens drilled around the circumference of the large diameter cores of the Lac du Bonnet granite (angle β) denote the fabric orientation within the intact rock in this case. The measured UCS and estimated CI and CD thresholds are shown in Fig. 18 and listed in Table 3. The CI threshold for the specimens is estimated from the lateral strain as well as the crack volumetric strain.

6.3 Olkiluoto Mica Gneiss

The variation of UCS for the Olkiluoto mica gneiss with respect to the fabric orientation (foliation angle)

approximately equal to 5.5 at the URL 420 level (see Table 1). The relaxation-induced micro-cracks (stress relief cracking) within rocks from this level are therefore expected to be horizontal. Specimens that
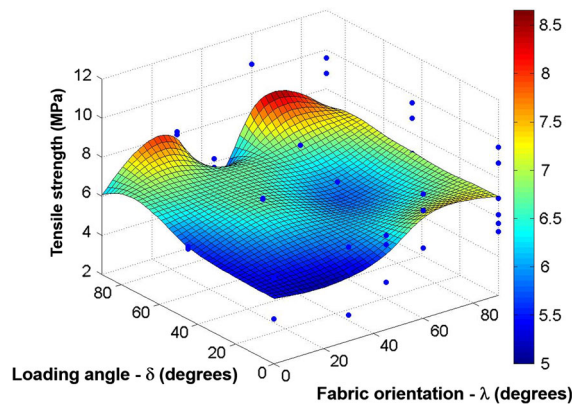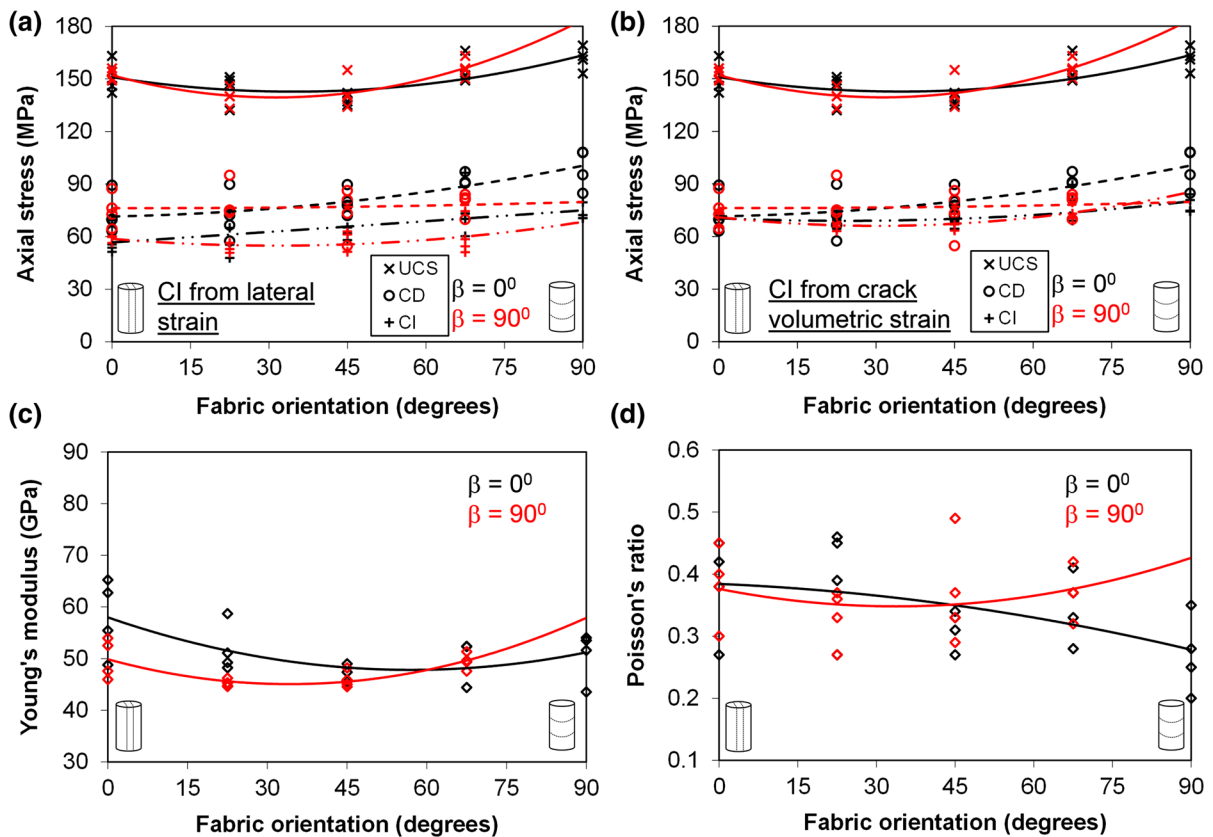
Fig. 17 Mechanical response of the Lac du Bonnet granite specimens studied for drilling-induced damage. *Solid, dashed* and *dash-dotted lines* in (**a**) and (**b**) are the second degree polynomial fits for the UCS, CD and CI thresholds, respectively;

a CI estimated from the lateral strain, **b** CI estimated from the crack volumetric strain, **c** Young's moduli and **d** Poisson's ratio, ($\beta = 0°$ data points are connected by the *black lines* and $\beta = 90°$ data points are connected by the *red lines*)

is illustrated in Fig. 19. The crack damage thresholds for the mica gneiss specimens were identified by using both AE and strain measurement methods. The extensometer measured strain data were used to determine CI and CD from the stresses associated with the maximum crack volumetric strain and volumetric strain within the strain approach, respectively. Since the number of specimens tested for each orientation is limited, the entire set of mica gneiss specimens was divided into three groups: 0°–30°, 30°–60° and 60°–90° with mean values for UCS, CI and CD shown in red markers for each group in Fig. 19. The reader is encouraged to consult Hakala et al. (2005) for a detailed investigation of the sensitivity of the tensile strength and elastic constants of the Olkiluoto mica gneiss to the foliation angle.

6.4 Queenston Shale

The measured UCS for the Queenston shale specimens are shown in Fig. 20. Calculated CI and CD thresholds for the vertical and horizontally laminated Queenston shale specimens are also presented in this figure. CI was identified from the onset of non-linearity of lateral strain and CD was estimated from the reversal point of the volumetric strain. Developing a conclusive anisotropy model is barely possible with such a limited number of specimens with different fabric orientations; however a useful comparison can be established for the Queenston shale behaviour with horizontal and vertical laminations with respect to the direction of major principal stresses. This will be further discussed in Sect. 7.

Table 3 The mean measured UCS and CI and CD thresholds estimated for the Lac du Bonnet granite specimens

Fabric orientation (°)	Coring damage (β = 0°/β = 90°)				Relaxation damage			
	UCS (MPa)	CD (MPa)	CI		UCS (MPa)	CD (MPa)	CI	
			Lat str*	Crk vol str**			Lat str*	Crk vol str**
0	151.3/152.3	72.9/75.2	57.4/59.1	70.9/71.1	152.3	75.2	59.1	71.1
22.5	144.8/139.8	71.4/79.6	60.8/54.0	69.2/66.0	149.0	77.6	59.6	71.2
45	138.5/142.5	79.8/73.7	62.6/56.7	66.6/67.6	149.3	83.8	61.1	69.9
67.5	155.5/156.0	92.8/79.2	74.9/59.6	79.6/73.4	156.0	79.9	55.2	73.7
90	161.5/–	98.9/–	73.2/–	78.5/–	151.3	72.9	57.4	70.9

* CI estimated from the onset of non-linearity of the lateral strain–axial stress curve

** CI estimated from the reversal point on the crack volumetric strain curve
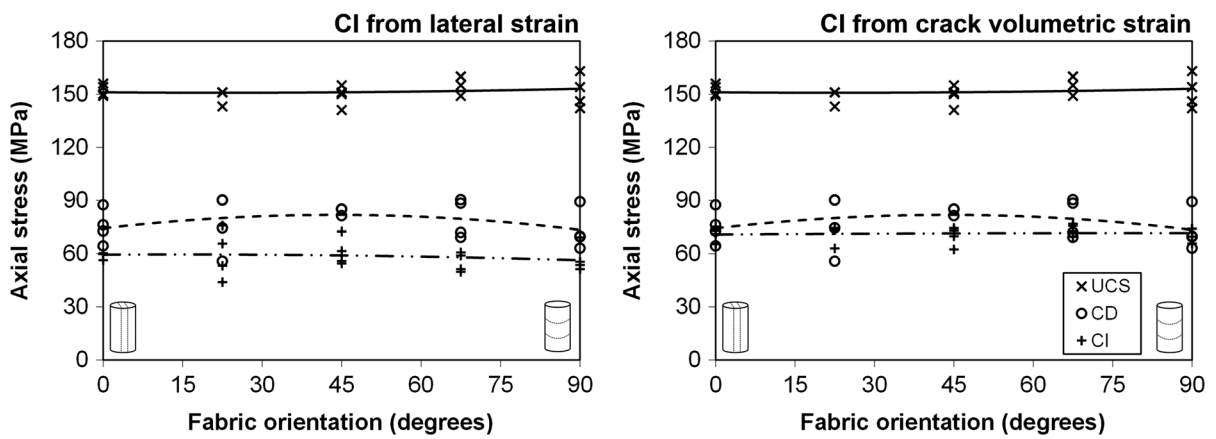

Fig. 18 UCS and crack damage thresholds for the Lac du Bonnet granite specimens studied for relaxation-induced damage. *Solid*, *dashed* and *dash-dotted lines* are the second degree polynomial fits for the UCS, CD and CI thresholds, *Left* CI is estimated from the lateral strain, *Right* CI is estimated from the crack volumetric strain

The wide distribution of peak strengths for the Queenston shale, independent of the fabric orientation (Fig. 20), can be mainly attributed to the difference in the silt fraction of the specimens. Grain size analysis data of the tested 90° specimens, provided to the authors courtesy of OPG, indicate the presence of claystones (shale) as well as siltstones in the specimens. Evaluation of the test results in Fig. 21 shows that an increase in the silt fraction of the Queenston shale improves its mechanical strength. With increasing silt fraction from 20 % (80 % shale) to 85 % (15 % shale) in the Queenston shale specimens the strength increases approximately six times and the Young's modulus increases approximately three times. These values can also be used as approximate indicators for the strength and stiffness contrast ratios

of the siltstone to claystones (shale) in the Queenston shale. It can be deduced from Fig. 21 that the shale content is controlling the CI limit while the CD threshold is controlled directly by the siltstone content of the specimens. Shale in the Queenston shale acts as the nucleation point and is an instigator for the initiation of new cracks, and as shown in Fig. 21, as long as approximately 30 % of the Queenston shale specimen is composed of shale (70 % siltstone), its CI threshold will remain constant or slightly decrease with increasing shale content. It can also be observed in this figure that the increase in the siltstone content of the Queenston shale specimens increases the crack propagation threshold. Therefore it can be concluded that in the Queenston shale, the shale (claystones) is the weakest link and is the nucleation point for new
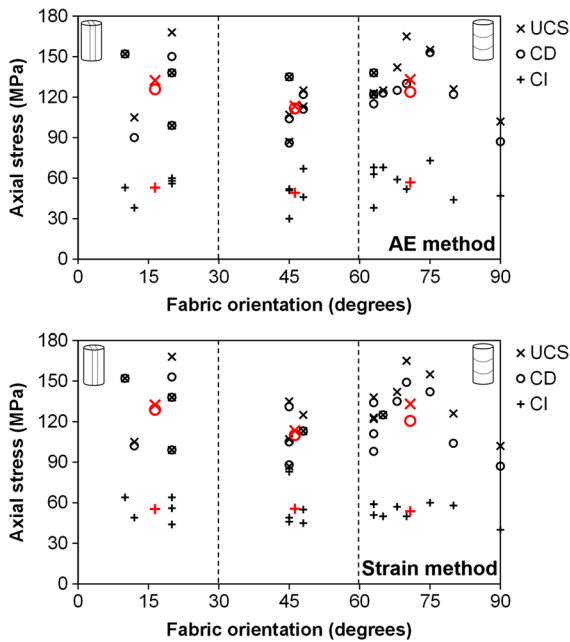
Fig. 19 UCS and CI and CD thresholds estimated from the AE and strain methods for the Olkiluoto mica gneiss; the mean values are shown with *red markers* (data from Hakala et al. 2005)
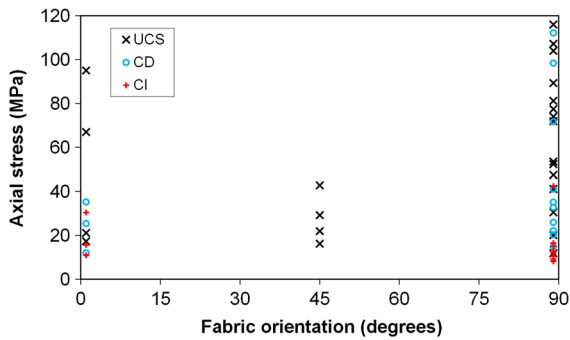

Fig. 20 Measured UCS and CI and CD thresholds estimated from the strain data for the Queenston shale

cracks. These cracks are suppressed by the available siltstone, similar to the mechanism that gravels in concrete deviate or suppress the fractures initiated within the cement matrix. As long as a minimum amount of shale exists, fractures will nucleate, and therefore increasing the shale content does not drastically decrease the CI threshold. However with increasing siltstone content, the ability of the Queenston shale to suppress fractures improves and consequently the CD limit increases.
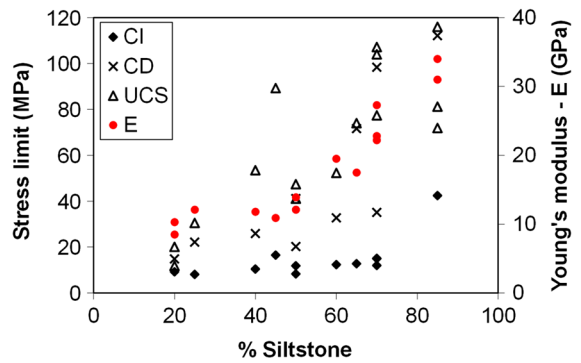

Fig. 21 Effect of silt fraction in the Queenston shale specimens with horizontal lamination on their mechanical properties

7 Discussion

The Cobourg limestone demonstrates the maximum and minimum peak strengths for the specimens with a fabric orientation of 90° (ranging approximately between 80 and 110 MPa with average UCS of 93.3 MPa) and 0° (ranging approximately between 40 and 80 MPa with average UCS of 60.8 MPa), respectively (see Fig. 11; Table 2). The peak strengths for the specimens with a vertical fabric (0°) are scattered over a range with minimum values close to the mean CI. This is consistent with Diederichs (2000), Diederichs et al. (2004) and Ghazvinian et al. (2012b) which describe CI as the true material property, while UCS is dependent upon the testing conditions (e.g. specimen geometry, specimen size, loading rate etc.) and can vary within a range, with the minimum equal to CI. The CD thresholds for the Cobourg limestone follow a similar trend as the peak strength, whereby the crack propagation stress limit changes from approximately 45–73 MPa for different fabric orientations as estimated from the AE data (Table 2).

A slim U-shaped anisotropic trend can be observed for the CI thresholds estimated from the AE data for the Cobourg limestone, with the maximums occurring at the 0° (with average CI of 35.5 MPa) and 90° (with average CI of 43.8 MPa) fabric orientations, and the minimum occurring at the 45° orientation (with average CI of 24.4 MPa). However, the slim U-shaped anisotropy is uncertain due to the heterogeneous nature of the Cobourg limestone at the investigated scale. While no direct measurement of strength and stiffness for the dark grey fine-grained argillaceous

bands and the light grey coarse-grained matrix of the Cobourg limestone exists, investigation of the UCS and Young's modulus of different rock classes with different mineralogies from the Cobourg formation by Perras (2014) results in an approximate measure of 1.25 and 1.4 for the strength and stiffness ratios of the light grey matrix to the dark grey argillaceous bands in the Cobourg limestone, respectively. The small values for the strength and stiffness contrast and undulating nature of nodule boundaries in the Cobourg limestone contribute to reducing the sensitivity of the CI threshold to the fabric orientation.

Laboratory testing or numerical modelling studies of core discing by many researchers, such as Dyke (1989) and Li and Schmitt (1998), show that the maximum damage to the rock occurs when the coring is aligned with the direction of the minor principal stress. Despite this, some damage was anticipated to occur within the large (20 cm) Lac du Bonnet granite cores that were bored within a close range to the orientation of the intermediate principal stress (σ_2). The assumption for choosing the fabric orientation of the Lac du Bonnet specimens in Sect. 6.2.1 was that the micro-fracturing in the rock occurs perpendicularly to the boring axis. The results in Fig. 17 show the anisotropic effect of the preferential orientation of pre-existing damage on the UCS of the specimens. The minimum and maximum mean UCS for specimens from the $\beta = 0°$ group occurs at 45° (138.5 MPa) and 90° (161.5 MPa), respectively (Table 3). The CD thresholds for the specimens in Fig. 17 are either independent ($\beta = 0°$) or increasing with increasing fabric orientation ($\beta = 90°$). The magnitude of the CD thresholds that are estimated here from the maximum volumetric strain are observed to be too low to compare to other references, i.e. 100.4 ($\pm$12.2) MPa from Table 1 (Martin 1993; Eberhardt 1998; Everitt 2001). The trend lines for the CI thresholds estimated from the crack volumetric strain for $\beta = 0°$ and 90° closely overlap and follow a nearly isotropic trend. The CI values estimated from the lateral strain method are always smaller than those estimated from the crack volumetric strain method (Table 3). The lateral strain CI thresholds for specimens belonging to the $\beta = 0°$ group have a linear trend line (increasing trend with increasing fabric orientation) while the trend line for when $\beta = 90°$, follows a moderate U-shape trend.

The Lac du Bonnet granite specimens investigated for relaxation-induced damage in Sect. 6.2.2 represent a perfect isotropic behaviour for UCS and CI thresholds estimated either from lateral strain or crack volumetric strain methods. The unusual behaviour of the CD thresholds where the maximum occurs at the 45° fabric orientation could have been attributed to the wrong selection of fabric orientation reference (i.e. by 45° offset). However the isotropic behaviour of the specimen at the CI threshold and the peak strength suggests that the CD threshold should also represent a similar isotropic behaviour. The up-side down U-shape trend is attributed to measurement or estimation error. The isotropic behaviour of the specimens in Fig. 18 can be justified either by accepting that relaxation-induced damage did not affect the cored material, or the fact that the preferred orientation of the pre-existing crack damage in rock has no effect on the mechanical response of the rock, which contradicts the previous discussion about the anisotropic behaviour observed in Fig. 17.

The dependency of the UCS and CD threshold (estimated from the AE and strain method) to the orientation of the fabric available in the Olkiluoto mica gneiss specimens can be observed in Fig. 19. The CI threshold, on the other hand, appears to be independent of the fabric orientation or insignificantly sensitive to foliation dipping when estimated by the AE method (Fig. 19). According to Shea and Kronenberg (1993), in metamorphic rocks with low mica content (less than approximately 20 % mica content, similar to the mica content of the investigated Olkiluoto mica gneiss), significant inelastic strains are accommodated mainly by extensive micro-cracking of the quartzo-feldspathic framework, and the role of ductile basal gliding and frictional sliding along cleavage in individual mica grains or at inter-granular boundaries within mica clusters isolated within a matrix of stronger silicates is negligible. With increasing mica content in a metamorphic rock, dislocation glide and frictional sliding along basal cleavage and kinking of mica grains accommodate the localized strains. However the increase in the mica content is associated with the transition of the mechanical behaviour of the rock from brittle to ductile (Shea and Kronenberg 1993) for which the discussion of CI and crack propagation is not critical. Mica with basal planes inclined to the orientation of the maximum principal stress can act as isolated shear flaws or as interacting flaws, depending upon the overlap and spacing of neighboring micas relative to their lengths, and may be able to generate significant stress

concentrations and nucleate fractures near their ends within the surrounding phases (Tapponnier and Brace 1976; Wong and Biegel 1985; Gottschalk et al. 1990; Shea and Kronenberg 1993). This said, the micas in low mica content rocks are isolated within the quartz, feldspar and other abundant phases that are distributed randomly and deform solely by micro-cracking. The nucleation of cracks within the homogenous quartzo-feldspathic framework (strong silica matrix) is the key for independency of the CI threshold to the orientation of fabric in gneissic rocks with low mica content (mica minerals are assumed to be the weakest links and are usually elongated in the foliation direction). At the crack propagation and interaction stress level, the quartzo-feldspathic bridges connecting the mica grains are arrayed in an en-echelon pattern, which introduce a dependency of the CD threshold to the foliation angle.

The limited test data available for different fabric orientations for the Queenston shale constrains the possibility for reaching a concluding remark for CI and CD anisotropy for this rock. However, the data will allow for the comparison of CI and CD thresholds for the two cases where the major principal stress is either parallel or perpendicular to the lamination. The CI limits for 0° and 90° Queenston shale specimens are observed to be within a very close range in Fig. 20, however they demonstrate significantly different ranges for the CD stress limits. This suggests that although the long term in situ strength of the Queenston shale with horizontal and vertical laminations with respect to the major principal stress will be similar, the short term in situ strength (e.g. during the construction period) or yielding strength of the 0° specimens (lamination parallel to the orientation of major principal stress) is lower than those of 90° specimens (horizontal lamination). The comparison of crack damage thresholds for the 0° Queenston shale specimens reveals that the CI and CD limits for these specimens are in a very close range. In another words, in Queenston shale samples with lamination parallel to orientation of major principal stress, as soon as fractures initiate, they become unstable, propagate and lead the specimen to failure.

8 Conclusions

The textural and/or structural planar fabric that exists in intact rocks controls the anisotropic behaviour of

the rock at different damage stress levels (CI, CD and UCS) depending on the fabric type (Fig. 4). Distinct types of fabric were investigated in this study through laboratory studies of the Cobourg limestone, grey Lac du Bonnet granite, Olkiluoto mica gneiss and Queenston shale.

The dark gray argillaceous bands could act as a minor micro-fracturing instigator in the Cobourg limestone while the alternating layers of packstone and argillaceous lime-mudstone wisps facilitate the interaction and coalescence of fractures. Therefore the fabric in the Cobourg limestone (Figs. 4d, h), considering the heterogeneity at the scale investigated, was observed to control the peak strength and CD threshold and to a lesser extent the CI stress limit of this rock. The type of fabric in the Lac du Bonnet granite is defined by the preferential orientation of pre-existing micro-fractures (Fig. 4g). The available test data for this rock showed that the fabric has minimal effect on CI thresholds, some control over the CD threshold and a key role in the anisotropic strength of specimens in terms of their peak strength. The UCS and CD threshold for the Olkiluoto mica gneiss are governed by the existing fabric (Figs. 4e, f), however the foliation does not play a significant role in controlling the CI threshold. The limited data available for the Queenston shale hampered the general conclusion regarding the effect of micro-scale layering on the fabric-guided micro-fracturing. However, the available data proved that the long term in situ strength (CI threshold) for this rock is impartial to the vertical or horizontal laminations with respect to the direction of the major principal stress while the fabric orientation is significant for the yielding strength (CD threshold) where specimens with laminations parallel to the major principal stress are weaker than the specimens with perpendicular laminations. Therefore while no firm anisotropic model can be established for the CI threshold, it can be deduced that UCS and CD threshold for the Queenston shale vary anisotropically with the fabric orientation.

The different fabric types investigated in this study were shown to control the CD thresholds and consequently the peak strength of the intact rocks. The fabrics represented by platy minerals, lenticular mineral aggregates or planar micro-fractures in an isotropic matrix (Olkiluoto mica gneiss and Lac du Bonnet granite) were shown to be non-essential to the CI threshold while no specific conclusion could be

established for the effect of micro-scale depositional layering of different mineral compositions (Queenston shale). The fabric defined by banding (spatial variation of grain sizes) with stiffness and strength contrast between the layers (Cobourg limestone), exhibited minor sensitivity of the CI stress level to the available fabric.

References

Amadei B (1996) Importance of anisotropy when estimating and measuring in situ stress in rock. Int J Rock Mech Min Sci Geomech Abstr 33(3):293–325

Amann F, Ündül Ö, Kaiser PK (2014) Crack initiation and crack propagation in heterogeneous sulfate-rich clay rocks. Rock Mech Rock Eng 47(5):1849–1865

ASTM (2012) Designation D7012-10: standard test method for compressive strength and elastic moduli of intact rock core specimens under varying states of stress and temperatures. ASTM International, West Conshohocken (PA)

Attewell PB, Sandford MR (1974) Intrinsic shear strength of a brittle, anisotropic rock—I: experimental and mechanical interpretation. Int J Rock Mech Min Sci Geomech Abstr 11(11):423–430

Barla G (1974) Rock anisotropy: theory and laboratory testing. In: Muller L (ed) Rock Mechanics. Springer, Wien, pp 131–169

Barron K (1971) Brittle fracture initiation in and ultimate failure of rocks: part III—anisotropic rocks: experimental results. Int J Rock Mech Min Sci Geomech Abstr 8(6):565–575

Bieniawski ZT (1967) Mechanism of brittle rock fracture: part II—experimental studies. Int J Rock Mech Min Sci Geomech Abstr 4(4):407–423

Brace WF, Paulding BW, Scholz C (1966) Dilatancy in the fracture of crystalline rocks. J Geophys Res 71(16):3939–3953

Brogly PJ, Martini IP, Middleton GV (1998) The Queenston Formation: shale dominated, mixed terrigenous-carbonate deposits of Upper Ordovician, semi-arid, muddy shores in Ontario, Canada. Can J Earth Sci 35(6):702–719

Colak K, Unlu T (2004) Effect of transverse anisotropy on the Hoek–Brown strength parameter 'mi' for intact rocks. Int J Rock Mech Min Sci 41(6):1045–1052

Dan DQ, Konietzky H, Herbst M (2013) Brazilian tensile strength tests on some anisotropic rocks. Int J Rock Mech Min Sci 58:1–7

Diederichs MS (2000) Instability of hard rock masses: the role of tensile damage and relaxation. Ph.D .Thesis, University of Waterloo, Waterloo, Ontario

Diederichs MS (2003) Rock fracture and collapse under low confinement conditions. Rock Mech Rock Eng 36(5):339–381

Diederichs MS (2007) The 2003 CGS geocolluquium address: damage and spalling prediction criteria for deep tunnelling. Can Geotech J 44(9):1082–1116

Diederichs MS, Kaiser PK, Eberhardt E (2004) Damage initiation and propagation in hard rock during tunnelling and the influence of near-face stress rotation. Int J Rock Mech Min Sci 41(5):785–812

Donath FA (1961) Experimental study of shear failure in anisotropic rocks. Geol Soc Am Bull 72(6):985–989

Dyke CG (1989) Core discing: its potential as an indicator of principal in situ stress directions. In: Proceedings of ISRM international symposium. International society for rock mechanics, Pau, France

Eberhardt E (1998) Brittle rock fracture and progressive damage in uniaxial compression. Ph.D. Thesis, Department of Geological Sciences, University of Saskatchewan, Saskatoon, p 334

Everitt RA (2001) The influence of rock fabric on excavation damage in the Lac du Bonnet granite. Ph.D. Thesis, University of Manitoba

Everitt RA, Brown A, Davison CC, Gascoyne M, Martin CD (1990) Regional and local setting of the Underground Research Laboratory. In: Proceedings of international symposium on unique underground structures, Denver, vol 2, pp 1–23

Gartner Lee (2008) Phase I regional geology, Southern Ontario. Supporting technical report, OPG 00216-REP-01300-00007-R00

Gatelier N, Pellet F, Loret B (2002) Mechanical damage of an anisotropic porous rock in cyclic triaxial test. Int J Rock Mech Min Sci 39(3):335–354

Ghazvinian E, Diederichs MS, Martin CD (2012a) Identification of crack damage thresholds in crystalline rock. In: Proceedings of Eurock 2012, Stockholm, Sweden

Ghazvinian E, Perras M, Diederichs M, Labrie D (2012b) Formalized approaches to defining damage thresholds in brittle rock: granite and limestone. In: Proceedings of the 46th US rock mechanics symposium, Chicago, USA

Gottschalk RR, Kronenberg AK, Russell JE, Handin J (1990) Mechanical anisotropy of gneiss: failure criterion and textural sources of directional behavior. J Geophys Res 95(B13):21613–21634

Hakala M, Heikkila E (1997) Laboratory testing of Olkiluoto mica gneiss in borehole OL-KR10. Posiva working report 97-07e

Hakala M, Kuula H, Hudson J (2005) Strength and strain anisotropy of Olkiluoto mica gneiss. Posiva working report 2005-61

Herget G, Arjang B (1990) Update on ground stresses in the Canadian Shield. In: Proceedings of stresses in underground structures (CANMET speciality conference), Ottawa, Canada, pp 33–47

Hobbs BE, Means WD, Williams PF (1976) An outline of structural geology, vol 570. Wiley, New York

Hoek E (1964) Fracture of anisotropic rock. J S Afr Inst Min Metall 64(10):501–518

International Society for Rock Mechanics Commission on Standardization of Laboratory and Field Tests (1978) Suggested methods for determining tensile strength of rock materials. Int J Rock Mech Min Sci 15(3):99–103

International Society for Rock Mechanics Commission on Standardization of Laboratory and Field Tests (1999) Suggested method for the complete stress–strain curve for intact rock in uniaxial compression. Int J Rock Mech Min Sci 36(3):279–289

Jaeger JC (1960) Shear failure of anisotropic rocks. Geol Mag 97(01):65–72

Jaeger JC, Cook NGW (1963) Pinching-off and disking of rocks. J Geophys Res 68(6):1759–1765

Karr DG, Law FP, Fatt MH, Cox GF (1989) Asymptotic and quadratic failure criteria for anisotropic materials. Int J Plast 5(4):303–336

Li Y, Schmitt DR (1998) Drilling-induced core fractures and in situ stress. J Geophy Res: Solid Earth 103(B3):5225–5239

Lim SS, Martin CD (2010) Core disking and its relationship with stress magnitude for Lac du Bonnet granite. Int J Rock Mech Min Sci 47(2):254–264

Martin CD (1993) The strength of massive Lac du Bonnet granite around underground openings. Ph.D. Thesis, Department of Civil and Geological Engineering, University of Manitoba, Winnipeg, MB

Martin CD (1997) Seventeenth Canadian geotechnical colloquium: the effect of cohesion loss and stress path on brittle rock strength. Can Geotech J 34(5):698–725

Martin CD, Read RS, Martino JB (1997) Observations of brittle failure around a circular test tunnel. Int J Rock Mech Min Sci 34(7):1065–1073

Martin CD, Kaiser PK, McCreath DR (1999) Hoek–Brown parameters for predicting the depth of brittle failure around tunnels. Can Geotech J 36(1):136–151

Martino JB, Thompson PM (1997) Status of the development of the deep doorstopper gauge system for in situ stress determination and summary of results from the deep stress measurement borehole at the Underground Research Laboratory. Ontario Hydro, Nuclear waste management division report 06819-REP-01200-10031-R00

Martino JB, Thompson PM, Chandler NA, Read RS (1997) The in situ stress program at AECL's Underground Research Laboratory. Ontario Hydro, Nuclear waste management division report 06819-REP-01200-0053-R00

Mazurek M (2004) Long-term used nuclear fuel waste management: geoscientific review of the sedimentary sequence in southern Ontario. Nuclear Waste Management Organization, Technical report TR 04-01

McLamore R, Gray KE (1967) The mechanical behavior of anisotropic sedimentary rocks. J Manuf Sci Eng 89(1):62–73

Nicksiar M, Martin CD (2013) Crack initiation stress in low porosity crystalline and sedimentary rocks. Eng Geol 154:64–76

Obert L (1977) The microseismic method-discovery and early history. In: Proceedings of first conference in acoustic

emission/microseismic activity in geologic structures and materials. Trans Tech Publications, Clausthal, Germany, pp 11–12

Obert L, Stephenson DE (1965) Stress conditions under which core disking occurs. Soc Min Eng 232(3):227–235

Pariseau WG (1972) Plasticity theory for anisotropic rocks and soils. In: Proceedings of the 10th US symposium on rock mechanics (USRMS), American Rock Mechanics Association

Passchier CW, Trouw RAJ (2005) Microtectonics, 2nd edn. Springer, Berlin

Peng SD (1971) Stresses within elastic circular cylinders loaded uniaxially and triaxially. Int J Rock Mech Min Sci Geomech Abstr 8(5):399–432

Peng S, Johnson AM (1972) Crack growth and faulting in cylindrical specimens of Chelmsford granite. Int J Rock Mech Min Sci Geomech Abstr 9(1):37–86

Perras MA (2009) Tunnelling in horizontally laminated ground: the influence of lamination thickness on anisotropic behavior and practical observations from the Niagara Tunnel Project. M.Sc. Eng. Thesis, Queen's University, Kingston, Ontario, Canada

Perras MA (2014) Understanding and predicting excavation damage in sedimentary rocks: a continuum based approach. Ph.D. Thesis, Queen's University, Kingston, Ontario, Canada

Ramamurthy T (1993) Strength, modulus responses of anisotropic rocks. In: Hudson JA (ed) Compressive rock engineering, vol 1. Pergamon, Oxford, pp 313–329

Read RS, Martin CD (1996) Technical summary of AECL's mine-by experiment phase I: excavation response. Atomic Energy of Canada Ltd., Pinawa, MB (Canada). Whiteshell Labs

Rigbey SJ, Huang JHS, Yuen CMK, Boase MH (1994) Exploratory adit program for the Niagara River Hydroelectric development. In: Proceedings of the 12th Canadian tunnelling conference

Schandl E (2009) Petrography of DGR-1 and DGR-2 core. NWMO technical report, TR-07-12

Schneider CA, Rasband WS, Eliceiri KW (2012) NIH image to imagej: 25 years of image analysis. Nat Methods 9(7):671–675

Shea WT, Kronenberg AK (1992) Rheology and deformation mechanisms of an isotropic mica schist. J Geophys Res: Solid Earth 97(B11):15201–15237

Shea WT, Kronenberg AK (1993) Strength and anisotropy of foliated rocks with varied mica contents. J Struct Geol 15(9):1097–1121

Stacey TR (1982) Contribution to the mechanism of core discing. J S Afr Inst Min Metall 82:269–275

Tapponnier P, Brace WF (1976) Development of stress-induced microcracks in Westerly granite. Int J Rock Mech Min Sci Geomech Abstr 13(4):103–112

Thompson PM, Chandler NA (2004) In situ rock stress determinations in deep boreholes at the Underground Research Laboratory. Int J Rock Mech Min Sci 41(8):1305–1316

Ündül Ö, Amann F, Aysal N, Plötze ML (2015) Micro-textural effects on crack initiation and crack propagation of andesitic rocks. Eng Geol. doi:10.1016/j.enggeo.2015.04.024

Vaittinen T, Ahokas H, Heikkinen E, Hellä P, Nummela J, Saksa P, Tammisto E, Paulamäki S, Paananen M, Front K, Kärki

A (2003) Bedrock model of Olkiluoto site, version 2003/1. Working report 2003-43. Posiva Oy, Olkiluoto

Walsh JB, Brace WF (1964) A fracture criterion for brittle anisotropic rock. J Geophys Res 69(16):3449–3456

Wong TF, Biegel R (1985) Effects of pressure on the micromechanics of faulting in San Marcos gabbro. J Struct Geol 7(6):737–749